minerals

MDPI

Article

Petrogenesis and Tectonic Setting of the Early and Middle Jurassic Granitoids in the Chaihe Area, Central Great Xing'an Range, NE China

Lu Shi [1], Nan Ju [1,2,*], Yuhui Feng [3], Changqing Zheng [4], Yue Wu [1] and Xin Liu [1]

[1] Shenyang Center of China Geological Survey, Shenyang 110034, China; shilu@mail.cgs.gov.cn (L.S.); wu.yue@mail.cgs.gov.cn (Y.W.); liuxin@mail.cgs.gov.cn (X.L.)
[2] College of Earth Sciences, China University of Geosciences, Beijing 100083, China
[3] College of Paleontology, Shenyang Normal University, Shenyang 110034, China; fyh@synu.edu.cn
[4] College of Earth Sciences, Jilin University, Changchun 130061, China; zhengchangqing@jlu.edu.cn
* Correspondence: junan@mail.cgs.gov.cn; Tel.: +86-181-0402-5767

Abstract: To ascertain the Early-to-Middle Jurassic tectonic setting in the central Great Xing'an Range, this study investigated the Early and Middle Jurassic granitoids exposed in the Chaihe area in the central Great Xing'an Range based on isotopic chronology and petrogeochemistry. The results of this study show that the Early and Middle Jurassic granitoids have emplacement ages of 179–172 Ma. Moreover, the Early and Middle Jurassic granitoids are high-K calc-alkaline unfractionated I-type granitoids and high-K calc-alkaline fractionated I-type granitoids, respectively. The magma sources of the Early and Middle Jurassic granitoids both originated from the partial melting of newly accreted lower crustal basaltic rocks. Meanwhile, the Middle Jurassic magma sources were mixed with mantle-derived materials or ocean-floor sediments formed by the dehydration and metasomatism of subducted slabs. The Early and Middle Jurassic granitoids in the study area were formed in the subduction environment of the oceanic crust, in which the Mongol-Okhotsk oceanic plate was subducted southward beneath the Eerguna and Xing'an blocks. Moreover, the Siberian plate began to collide and converge with northeast China during the Middle Jurassic.

Keywords: central Great Xing'an Range; Early and Middle Jurassic; granitoids; petrogenesis; southward subduction of the Mongol-Okhotsk oceanic plate

Citation: Shi, L.; Ju, N.; Feng, Y.; Zheng, C.; Wu, Y.; Liu, X. Petrogenesis and Tectonic Setting of the Early and Middle Jurassic Granitoids in the Chaihe Area, Central Great Xing'an Range, NE China. *Minerals* **2023**, *13*, 917. https://doi.org/10.3390/min13070917

Academic Editor: Jaroslav Dostal

Received: 22 May 2023
Revised: 4 July 2023
Accepted: 5 July 2023
Published: 7 July 2023

1. Introduction

The Great Xing'an Range of China is located in the eastern part of the Central Asian Orogenic Belt (CAOB) between the Siberian Craton in the north and the North China Craton in the south [1–8]. It has been suggested that this orogenic segment has undergone two stages of tectonic evolution, of which the earlier stage was related to the subduction and closure of the Paleo-Asian Ocean [9–15], whereas the later stage was related to the subduction of the Pacific Ocean [16–19]. Volcanic rocks and granitoids are widely distributed throughout the Great Xing'an Range, and an understanding of the timing and stages of emplacement of these granitoids is critical for reconstructing the tectonic and magmatic evolution of northeastern China. A large number of existing studies have found that most of the volcanic rocks and granitoids in the region were emplaced during Mesozoic time, with only a few during Neoproterozoic and Paleozoic times [20–22].

The Late Mesozoic volcanic rocks and granitoids in the Great Xing'an Range are an important part of the large-scale Late Mesozoic magmatism in northeast China. Their petrogenesis and tectonic setting have been hot research topics for geologists. However, the tectonic setting of the large-scale Late Mesozoic magmatic rocks in northeast China remains controversial and is believed to be related mainly to (1) the mantle plume structure [23]; (2) the closure and post-orogenic collapse of the Mongol-Okhotsk Ocean [24,25]; (3) the

subduction of the Paleo-Pacific plate [26]; and (4) both the closure of the Mongol-Okhotsk Ocean and the subduction of the Paleo-Pacific plate [27]. The interaction mode related to the mantle plume structure can almost be excluded based on the non-annular distribution of volcanic rocks in the Great Xing'an Range and its adjacent areas [24,28]. However, no consensus has been reached on the other three views. The central Great Xing'an Range, located between the Mongol-Okhotsk tectonic belt in the northwest and the Paleo-Pacific plate in the east, is a key area for research on this scientific problem. Therefore, it is necessary to conduct a systematic and in-depth study of the Early-Middle Jurassic granitic rocks in the central Great Xing'an Range. Based on field geological surveys, this study investigated the Early-Middle Jurassic granitic rocks exposed in the study area through systematic petrological, geochronological, and petrogeochemical studies. Accordingly, this study determined the petrogenetic characteristics of these granitic rocks and explored their tectonic setting.

2. Geological Setting and Geological Characteristics of Plutons

The Great Xing'an Range lies in the Xing'an-Mongolian orogenic belt, east of the Central Asian Orogenic Belt. In terms of geotectonic position, it is located between the Siberian and North China Cratons (Figure 1) [29,30]. From the end of the Paleozoic to the Early Mesozoic, with the collision and convergence of several microblocks such as Eerguna, Xing'an, and Songnen [1,20], the Paleo-Asian Ocean was completely closed, and the southern part of the Xing'an-Mongolian orogenic belt and the North China plate collided and converged along the Xilamulun-Changchun-Yanji suture belt, forming a unified Asian continent [31]. Since the Jurassic, the tectonic framework of northeast China has undergone dramatic changes from EW-trending structures to NE- and NNE-trending structures, entering the evolutionary stage of the Circum-Pacific and Mongol-Okhotsk tectonic systems [32].

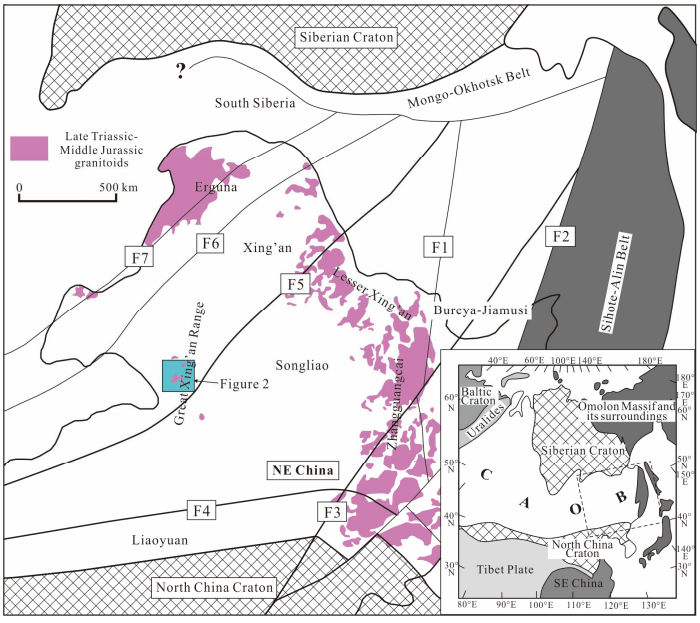

Figure 1. Tectonic map of NE China in the eastern CAOB (modified from references [29,30]) and the position of Figure 2. It consists of several microcontinental blocks and/or terranes, including the Jiamusi block and its northern extension in Bureya (Russia), the Songliao terrane, the Xing'an terrane, and the Erguna Massif. Major faults: F1: Mudanjiang fault; F2: Dunhua–Mishan Fault (northern branch of the Tanlu Fault); F3: Yitong–Jiamusi Fault; F4: Xar Moron–Changchun–Yanji Fault; F5: Hegenshan–Zhalantun–Heihe Fault; F6: Tayuan–Xiguitu Fault; F7: Derbugan–Southern Mongolia Fault.

The Chaihe area is located on the Xing'an block. The Late Mesozoic Jurassic-Cretaceous strata in this area are dominated by continental volcanic rocks and continental clastic sedimentary rocks. They primarily include the Middle Jurassic Wanbao Formation, the Upper Jurassic Tamulangou and Manketouebo formations, and the Lower Cretaceous Manitu, Baiyingaolao, Meiletu, and Damoguaihe formations. The Late Mesozoic intrusions were mainly active during the Early-to-Middle Jurassic (179–172 Ma), the Late Jurassic (152–149 Ma), and the Early Cretaceous (137–120 Ma) [21]. The Early and Middle Jurassic granitoids in the Chaihe area are distributed locally and mostly occur as stocks. Field surveys have revealed that these granitoids intrude into Paleozoic strata and are unconformably overlain by the volcanic rocks of the Late Jurassic Manketouebo Formation (Figure 2) [33]. Early Jurassic granitoids mainly include porphyritic quartz monzonites. The Middle Jurassic granitoids are dominated by monzogranites, with a small quantity of granodiorites and quartz monzonites. The details are shown in Table 1.

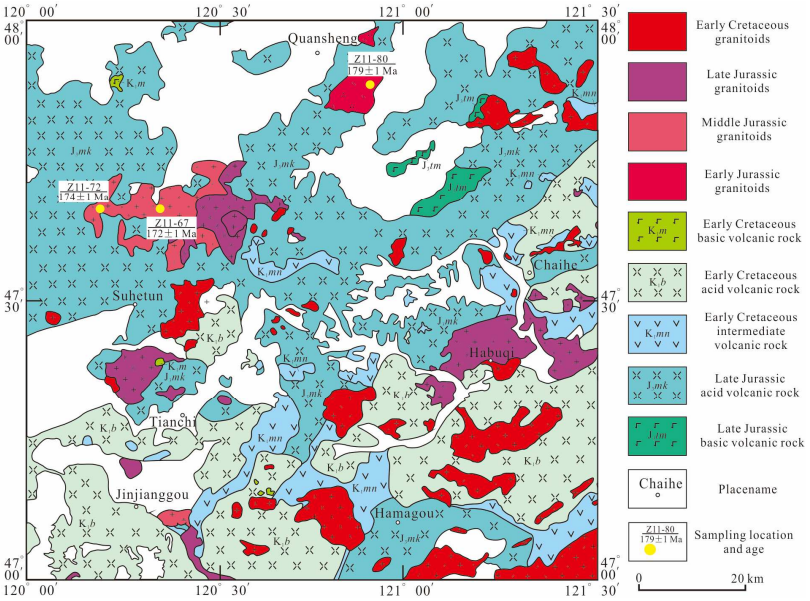

Figure 2. Geological sketch map of the Chaihe area in the central Great Xing'an Range (Modified from reference [33]).

Table 1. Petrographic features of the Early and Middle Jurassic granitoids in the Chaihe area.

Age	Rock Type	Texture	Mineral Content and Characteristics	Samples No.
Early Jurassic	Quartz monzonite	Porphyritic textures, about 70% phenocrysts and about 30% matrix with aplitic textures and massive structures	Quartz (15%±), plagioclase (45%±), alkali feldspars (35%±), and mafic minerals (5%±) such as primary biotite, augite, and secondary epidote (Figure 3a,b). The main types of plagioclase are andesine and labradorite. Quartz grains are anhedral, plagioclase grains show polysynthetic twins, and some alkali feldspar grains have Carlsbad twins.	Zircon U-Pb and Hf Isotope: Z11-80 Whole-Rock: Z11-80, B1245-1, B4239-2, B4239-3, B4241-1, B4246-1 B4246-2, B4247-1
Middle Jurassic	Quartz monzonite	Fine-grained granitic textures, and massive structures	Alkali feldspars (30%±), plagioclase (45%±), quartz (15%±), and a small amount of hornblende (5%±) and biotite (5%±). Their mafic minerals have undergone intense chlorite alteration and carbonation (Figure 3c,d).	

Table 1. *Cont.*

Age	Rock Type	Texture	Mineral Content and Characteristics	Samples No.
	Granodiorite	Medium-to fine-grained granitic textures, and massive structures	Alkali feldspar (15%±), plagioclase (45%±), quartz (28%±), and a small amount of mafic minerals (12%±) such as biotite and hornblende (Figure 3e,f). In addition, their accessory minerals include sphene, apatite, and magnetite. Quartz grains are anhedral, plagioclase grains have polysynthetic twins, and hornblende grains are generally euhedral.	
	Monzogranite	Medium- to fine-grained granitic textures, massive structures, and local cataclastic structures	Quartz (30%±), plagioclase (35%±), perthite (20%±), orthoclase (10%±), and biotite (5%±) (Figure 3g,h). Quartz grains are anhedral and fill between other mineral particles; perthite grains show striated twins; orthoclase grains have Carlsbad twins.	Zircon U-Pb and Hf Isotope: Z11-67, Z11-72 Whole-Rock: Z11-72, B1227-1 B3230-4, B3234-1

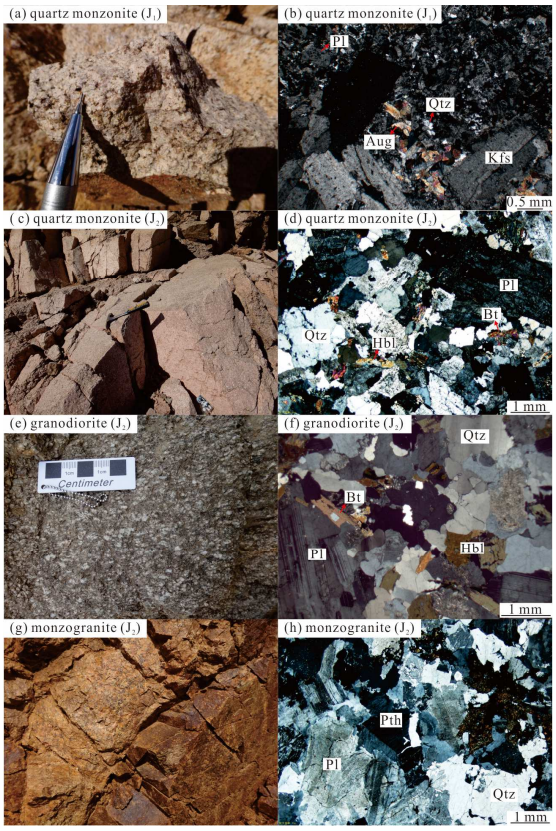

Figure 3. Field photographs and microphotographs of the Early and Middle Jurassic granitoids in the Chaihe area. (**a**) Field photograph of the Early Jurassic quartz monzonite; (**b**) Microphotograph of the Early Jurassic quartz monzonite; (**c**) Field photograph of the Middle Jurassic quartz monzonite; (**d**) Microphotograph of the Middle Jurassic quartz monzonite; (**e**) Field photograph of the Middle Jurassic granodiorite; (**f**) Microphotograph of the Middle Jurassic granodiorite; (**g**) Field photograph of the Middle Jurassic monzogranite; (**h**) Microphotograph of the Middle Jurassic monzogranite. Qtz—quartz; Pl—plagioclase; Kfs—k-feldspar; Pth—perthite; Aug—augite; Hbl—hornblende; Bt—biotite.

3. Analytical Methods

3.1. Zircon U-Pb Dating

Zircon U-Pb dating was performed on three selected samples: Z11-80 (Early Jurassic quartz monzonite), Z11-67, and Z11-72 (Middle Jurassic monzogranite). Zircons with sound crystal morphology and no or few fractures were selected from rock samples and placed in resin for preparing targets and polishing. The cathodoluminescence (CL) images of zircon were obtained at the Beijing SHRIMP Center, Chinese Academy of Geological Sciences. Zircon U-Pb dating was conducted at the Tianjin Institute of Geology and Mineral Resources using laser ablation inductively coupled plasma mass spectrometry (LA-ICP-MS), with a laser spot size of 35 μm and high-purity He being used as the carrier gas for denudation. In the calculations of Zircon ages, GJ-1 zircon reference material was employed as the external standard for isotopic fractionation corrections, and synthetic glass NIST SRM610 was used as the external standard for instrument optimization. The concordant ages of the samples were calculated using ISOPLOT (version 3.0).

3.2. In Situ Zircon Hf Isotope Analysis

On the basis of zircon U-Pb dating, in situ zircon Hf isotope analysis was performed at the Tianjin Institute of Geology and Mineral Resources using a multi-collector inductively coupled plasma mass spectrometer (MC-ICP-MS, NEPTUNE) and a 193-nm laser ablation system with a laser spot size of 50 μm. The detailed experiment and analysis process are stated in Geng et al. [34]. The decay constant of ^{176}Lu was set at 1.865×10^{-11} year^{-1} for calculation [35]. To calculate the $\varepsilon_{Hf}(t)$ values, the $^{176}Lu/^{177}Hf$ and $^{176}Hf/^{177}Hf$ ratios of the depleted mantle were set at 0.0384 and 0.28325, respectively [36]. The Hf model ages were calculated according to studies by Griffin et al. [36], Nowell et al. [37], and Amelin et al. [38].

3.3. Whole-Rock Major- and Trace-Element Analysis

Twelve fresh samples (eight Early Jurassic quartz monzonites and four Middle Jurassic monzogranites) were selected, washed, dried, and ground into powders (<200 mesh) for the analysis of major and trace elements. The analysis and tests were completed at the Tianjin Institute of Geology and Mineral Resources. The major elements were analyzed using X-ray fluorescence spectrometry (XRF) on fused glasses. Both Fe_2O_3 and FeO were analyzed by the potassium dichromate volumetric method. The trace elements were analyzed using inductively coupled plasma mass spectrometry (ICP-MS) after acid digestion of samples in Teflon bombs. Detailed sample preparation and analytical procedures followed Li et al. [39]. The precision of the major element analyses is within ±2% for the oxides greater than 0.5 wt.% and within ±5% for the oxides greater than 0.1 wt.%. The uncertainties for the trace element analyses are within 5%.

4. Analytical Results

4.1. Zircon U-Pb Ages

The zircon U-Pb dating results of the Early and Middle Jurassic granitoids are shown in Supplementary Table S1.

Sample Z11-80 is a porphyritic quartz monzonite, and 40 zircon grains in this sample were dated. These zircons are mostly short and prismatic, and some of them are granular, with grain sizes of 100–200 μm and length/width ratios of 1:1–2:1. The cathodoluminescence (CL) images (Figure 4a) show that these zircon grains have typical zonal textures and Th/U ratios of 0.3722–1.1914, suggesting magmatic zircons. All 40 zircons have highly concentrated U-Pb ages, except for one, which has a U-Pb age of 308 ± 2 Ma. As shown in the concordia diagram (Figure 4b), all the zircon U-Pb ages lie on or near the concordant curve, and the concordant age is obtained at 179 ± 1 Ma (MSWD = 1.4). This Early Jurassic age represents the emplacement age of quartz monzonite, and the age of 308 ± 2 Ma is the age when the zircon grain was trapped in or inherited by quartz monzonite.

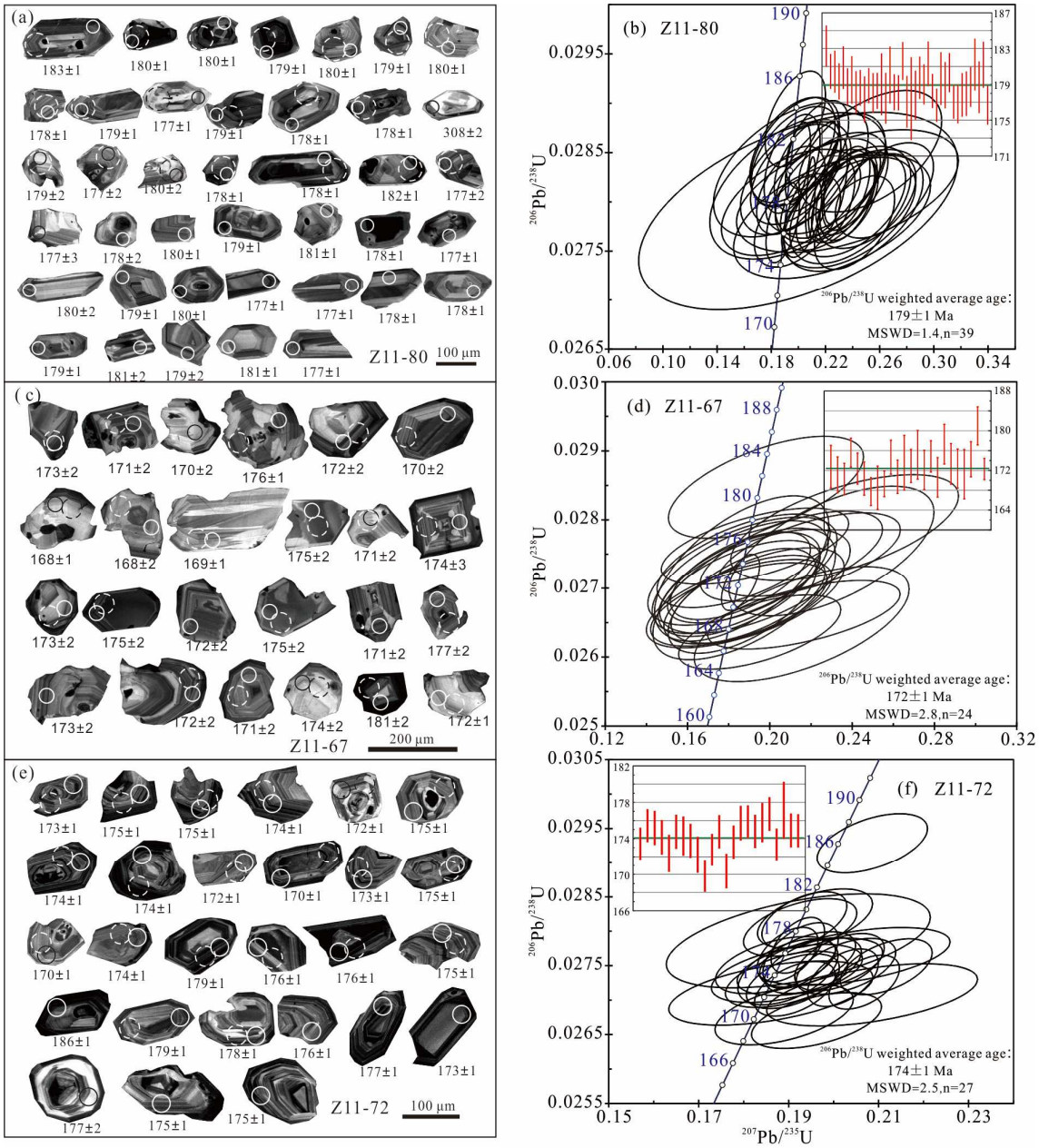

Figure 4. CL images and U-Pb age concordia diagrams of zircons from the Early and Middle Jurassic granitoids in the Chaihe area. (**a**) CL image of zircons from sample Z11-80, (**b**) Zircon U-Pb age concordia diagram from sample Z11-80, (**c**) CL image of zircons from sample Z11-67, (**d**) Zircon U-Pb age concordia diagram from sample Z11-67, (**e**) CL image of zircons from sample Z11-72, (**f**) Zircon U-Pb age concordia diagram from sample Z11-72. Note: solid circles indicate the positions for zircon U-Pb isotopic dating; dotted circles indicate positions for zircon Lu-Hf isotopic compositions.

Sample Z11-67 is a monzogranite, and 25 zircon grains in this sample were dated. These zircons are mostly short, prismatic, and granular, with grain sizes of 100–250 μm and length/width ratios of 1:1–2.5:1. The CL image (Figure 4c) shows that these zircons have typical zonal textures and Th/U ratios of 0.8121–1.5717, suggesting magmatic zircons. As shown in the concordia diagram (Figure 4d), all the zircon U-Pb ages are located on or near the concordant curve, with a weighted average $^{206}Pb/^{238}U$ age of 172 ± 1 Ma (MSWD = 2.8). This Middle Jurassic age represents the emplacement age of granites.

Sample Z11-72 is a monzogranite, and 27 zircon grains in this sample were dated. These zircons are mostly short prismatic and granular, with grain sizes of 70–150 μm and

length/width ratios of 1:1–3:1. The CL images (Figure 4e) show that these zircons have typical zonal textures and Th/U ratios of 0.7237–1.8152, suggesting magmatic zircons. As shown in the concordia diagram (Figure 4f), all the zircon U-Pb ages are located on or near the concordant curve, with a weighted average $^{206}Pb/^{238}U$ age of 174 ± 1 Ma (MSWD = 2.5). This Middle Jurassic age represents the emplacement age of granites.

4.2. In Situ Zircon Hf Isotopic Composition

Based on the LA-ICP-MS zircon U-Pb dating for the Early and Middle Jurassic granitoids in the study area, this study conducted in situ zircon Hf isotope analysis of some zircons from the dating samples. The analytical results are shown in Supplementary Table S2.

Twenty zircons that were taken from Early Jurassic quartz monzonite porphyry sample Z11-80 and represented the formation age of this sample had initial $^{176}Hf/^{177}Hf$ ratios of 0.282824–0.282956 and $\varepsilon_{Hf}(t)$ values of +5.64–+10.33 (weighted average: +7.09–0.59). They had single-stage Hf model ages T_{DM1} (Hf) and two-stage Hf model ages T_{DM2} (Hf) of 421–602 Ma and 515–775 Ma, respectively.

Twenty zircons from Middle Jurassic monzogranite sample Z11-67 had initial $^{176}Hf/^{177}Hf$ ratios of 0.282898–0.283064 and $\varepsilon_{Hf}(t)$ values of +8.12–+14.06 (weighted average: +9.51 ± 0.57). Their T_{DM1} (Hf) and T_{DM2} (Hf) ages were 268–508 Ma and 303–633 Ma, respectively. 20 zircons from Middle Jurassic monzogranite sample Z11-72 had initial $^{176}Hf/^{177}Hf$ ratios of 0.282856–0.282995 and $\varepsilon_{Hf}(t)$ values of +6.64–+11.55 (weighted average: +8.5 ± 0.66). Their T_{DM1} (Hf) and T_{DM2} (Hf) ages were 365–560 Ma and 440–715 Ma, respectively.

Overall, zircons of the Early and Middle Jurassic granitoids in the Chaihe area have positive $\varepsilon_{Hf}(t)$ values and young T_{DM2} (Hf) ages, which are concentrated in the Neoproterozoic and the Paleozoic. As shown in the $\varepsilon_{Hf}(t)$-t diagram (Figure 5) [40], the zircon Hf isotope data of the Early and Middle Jurassic granitoids all fall between the evolution lines of the depleted mantle and chondrite and within the eastern part of the Xing'an-Mongolian orogenic belt. This result indicates that the magmas of the Early and Middle Jurassic granitoids originate from newly accreted crustal materials. In addition, the Middle Jurassic granitoids have higher zircon $\varepsilon_{Hf}(t)$ values and approach the depleted mantle evolution line, suggesting that the Middle Jurassic magma source might be mixed with mantle-derived components.

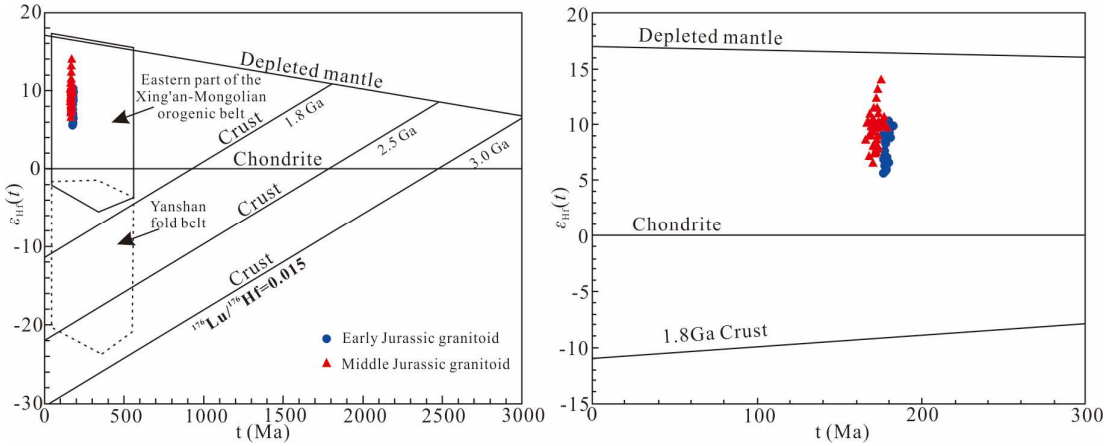

Figure 5. ε_{Hf}(t) vs. t diagrams of the Early and Middle Jurassic granitoids in the Chaihe area.

4.3. Major and Trace Elements

The analytical results of the whole-rock major and trace elements in the Early and Middle Jurassic granitoids in the study area are shown in Supplementary Table S3.

The Early Jurassic quartz monzonite samples from the Chaihe area have a SiO_2 content of 63.3%–67.85%, a TiO_2 content of 0.51%–0.803%, an Al_2O_3 content of 14.8%–16.3%, a FeO^T content of 3.01%–4.39%, a MgO content of 0.83%–1.74%, a CaO content of 1.66%–3.19%, a

Na_2O content of 4.20%–5.45%, and a K_2O content of 3.65%–4.17%. Their Na_2O/K_2O ratios are 1.09–1.43, indicating that they are relatively enriched in sodium (Na) and depleted in potassium (K). Their Rittmann index σ (3.00–4.22) suggests calc-alkaline—alkaline characteristics. As shown in the rock series discrimination diagram (Figure 6a), the samples all fall into the high-K calc-alkaline zone. Moreover, the rock samples have an aluminum saturation index A/CNK of 0.91–1.02 and fall into the meta-aluminous—weakly peraluminous zone in the A/CNK-A/NK diagram (Figure 6b).

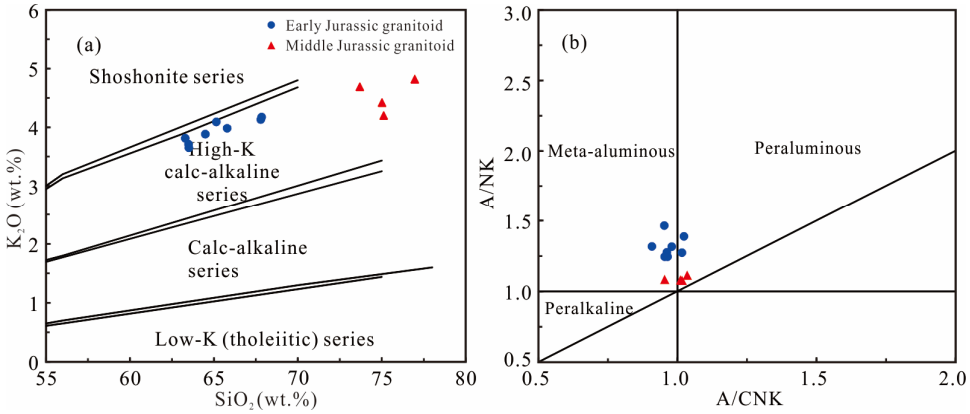

Figure 6. The SiO_2-K_2O rock series discrimination diagram ((**a**); [41,42]) and aluminum saturation index diagram ((**b**); [43]) of the Early and Middle Jurassic granitoids.

The Middle Jurassic monzogranites samples have a SiO_2 content of 73.70%–76.98%, a TiO_2 content of 0.13%–0.23%, an Al_2O_3 content of 12.18%–13.70%, a FeO^T content of 1.09%–1.54%, a MgO content of 0.18%–0.31%, a CaO content of 0.36%–0.86%, a Na_2O content of 3.7%–4.62%, and a K_2O content of 4.20%–4.82%. Their Na_2O/K_2O ratios are 0.77–1.03, indicating that they are relatively enriched in K and depleted in Na. Their Rittmann index σ (2.14–2.82) suggests calc-alkaline characteristics. As revealed by the rock series discrimination diagram (Figure 6a), the samples all fall into the high-K calc-alkaline zone. Moreover, the rock samples have an aluminum saturation index A/CNK of 0.95–1.04 and fall into the weakly peraluminous zone in the A/CNK-A/NK diagram (Figure 6b). CIPW norm mineral calculations for the Early and Middle Jurassic granitoids match modal abundances estimated by petrographic observation (Supplementary Table S3 and Figure 3).

As shown in the total alkali-silica (TAS) diagram of the rock samples (Figure 7) [44,45], the Early Jurassic quartz monzonite samples fall near the boundary between the zones of the alkaline and subalkaline series and are primarily projected into the zone of the subalkaline series. Therefore, these samples are primarily composed of quartz monzonite. The TAS diagram also shows that the Middle Jurassic granitoids samples are all projected into the subalkaline series zone, indicating that they were composed of granites. As shown in the Harker diagram (Figure 8), the Early-Middle Jurassic granitoids samples all showed significant correlations. Specifically, the TiO_2, Al_2O_3, FeO^T, CaO, MgO, Na_2O, and P_2O_5 contents decrease with an increase in the SiO_2 content, while the K_2O content and the K_2O/Na_2O ratio increase with an increase in the SiO_2 content. These results suggest that the magma evolution underwent the fractional crystallization of mafic minerals and plagioclase, implying that the Early and Middle Jurassic granitoids had the same (or similar) source rocks.

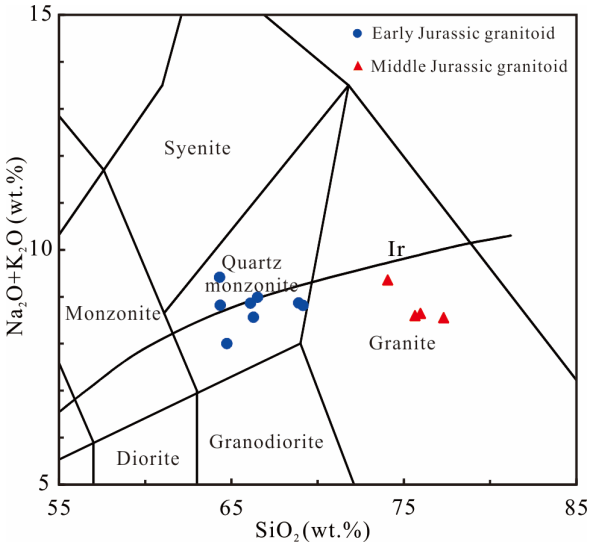

Figure 7. TAS diagram of the Early and Middle Jurassic granitoids in the Chaihe area [44,45]. Ir—Irvine dividing line between alkaline and subalkaline compositions. Above the line is the alkaline field; below is the subalkaline field.

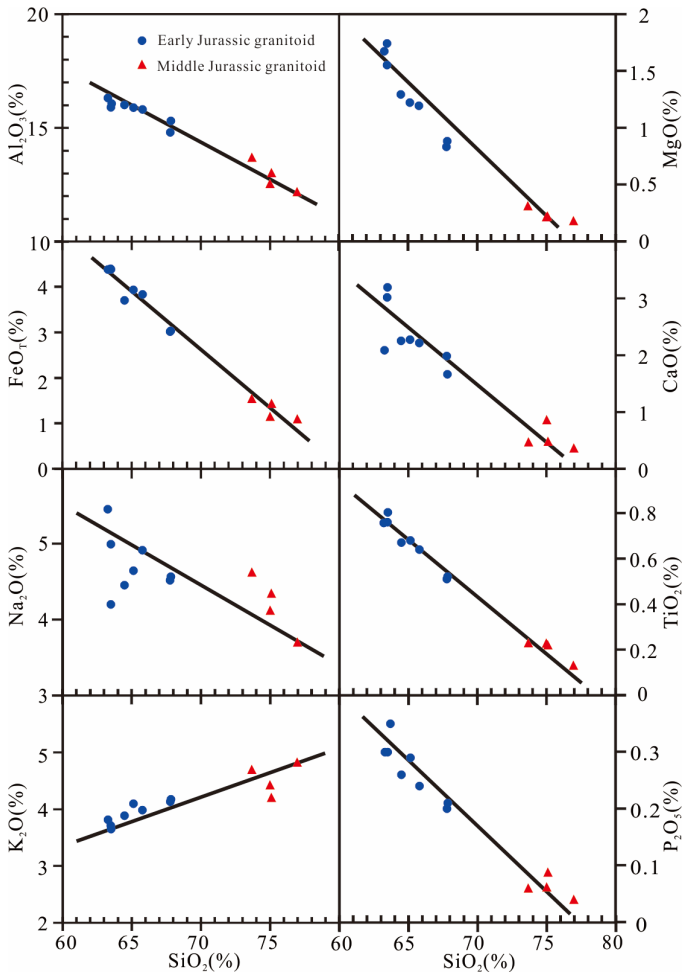

Figure 8. Harker diagram of the Early and Middle Jurassic granitoids in the Chaihe area.

As shown in the primitive mantle-normalized trace element spider diagram (Figure 9a), the Early Jurassic granitoids samples are relatively enriched in large-ion lithophile elements

(LILEs; e.g., Rb, U, K, and LREEs) and Zr and Hf and are depleted in high-field-strength elements (HFSEs; e.g., Nb, Ta, P, and Ti) and Sr. Similar to the Early Jurassic granitoids samples, the Middle Jurassic granitoids samples are also relatively enriched in LILEs (e.g., Rb, Th, U, K, and LREEs) and Zr and Hf and are depleted in HFSEs (e.g., Nb, Ta, P, and Ti) and Ba and Sr. However, the Early and Middle Jurassic granitoids samples exhibit significantly different degrees of enrichment and depletion of these elements. Specifically, the Middle Jurassic granitoids samples were more significantly depleted in Sr, P, and Ti; the Early Jurassic granitoids samples do not exhibit Ba anomalies, while the Middle Jurassic granitoids samples show strong negative Ba anomalies; and the Early Jurassic granitoids samples exhibit weakly negative Th anomalies, while the Middle Jurassic granitoids samples show significantly positive Th anomalies.

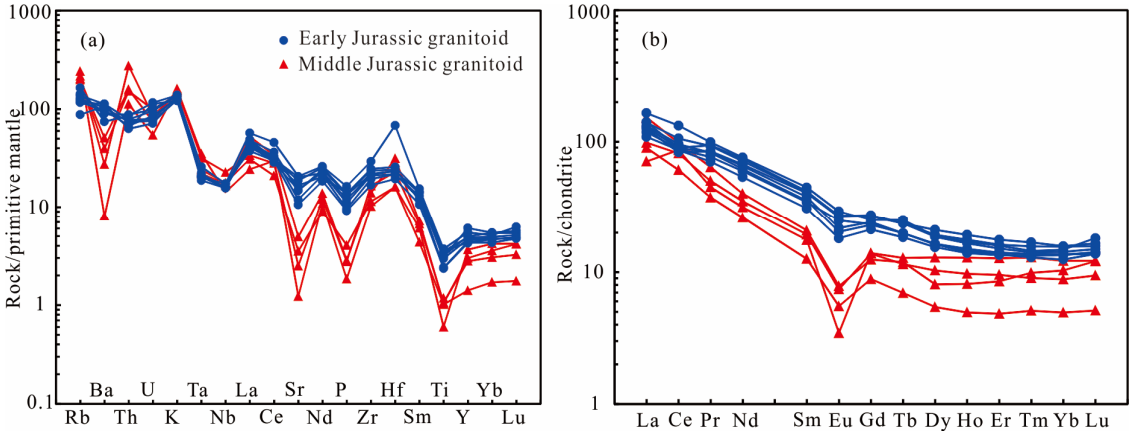

Figure 9. The primitive mantle-normalized trace element spider diagram (**a**) and chondrite-normalized REE patterns (**b**) of the Early and Middle Jurassic granitoids in the Chaihe area. The normalization values for the primitive mantle and chondrite are from reference [46].

The Early Jurassic granitoids samples have a total rare earth element (ΣREE) content of 130.85–191.02 μg/g, a LREE/HREE ratio of 6.59–9.74, an $(La/Yb)_N$ ratio of 7.92–11.12, and δEu values of 0.70–0.86. In contrast, the Middle Jurassic granitoids samples have a ΣREE content of 82.05–133.69 μg/g, a LREE/HREE ratio of 7.49–13.55, an $(La/Yb)_N$ ratio of 5.79–18.10, and δEu values of 0.22–0.51. As shown in the chondrite-normalized REE patterns (Figure 9b), the Early and Middle Jurassic granitoids samples exhibit similar rightward trends, suggesting that they are relatively enriched in LREEs and depleted in HREEs. Compared with the Early Jurassic granitoids samples, the Middle Jurassic granitoids samples have a lower ΣREE content, a higher LREE/HREE fractionation degree, and more significant negative Eu anomalies.

5. Discussion

5.1. Distribution of the Early and Middle Jurassic Granitoids in the Great Xing'an Range

The Early-to-Middle Jurassic magmatic activity in northeast China occurred primarily in the Great Xing'an Range and Manzhouli areas and the Lesser Xing'an Range–Zhangguangcai Range area at 198–164 Ma and 199–166 Ma [32], respectively, and is distributed locally in the Songliao Basin (granitic basement rocks) and the eastern areas of the Jilin and Heilongjiang provinces [32,47] (Figure 1). The Early and Middle Jurassic granitoids in the Great Xing'an Range are distributed mainly in the Eerguna block in the north, where many Early-to-Middle Jurassic granitic rocks have also been discovered [20]. The formation of these rocks is related to the subduction of the Mongol-Okhotsk oceanic plate beneath the Eerguna block. However, there are few reports on the Early and Middle Jurassic granitoids in the central Great Xing'an Range. According to the latest geological survey results, a few Early-to-Middle Jurassic granitic rocks are distributed in the central Great Xing'an Range, and most of them occur as small stocks. Ge et al. [48] identified the

Early-to-Middle Jurassic Dashizhai and Jingyang plutons in the Ulanhot area, which have zircon U-Pb ages of 174 ± 4 Ma and 182 ± 3 Ma, respectively. Wu et al. [20] concluded that no Jurassic plutons have been discovered in the Xing'an block in the central Great Xing'an Range but that Jurassic plutons with ages of 179–157 Ma are exposed in the Songnen block in the south. Yu et al. [49] discovered a set of Middle Jurassic granitoids with zircon ages of 173–166 Ma in the northern Taerqi area. This study revealed that the Early-to-Middle Jurassic granitic rocks in the study area had emplacement ages of 179–172 Ma. Since there are few Early-to-Middle Jurassic granitoids exposed in the central Great Xing'an Range, this new discovery of the Early-to-Middle Jurassic granitoids in the Chaihe area provides a solid foundation for research on the tectonic-magmatic evolution process in the Great Xing'an Range.

5.2. Petrogenesis of the Early and Middle Jurassic Granitoids

5.2.1. Petrogenetic Types of Granitoids

Granitoids can be commonly divided into I, S, M, and A types based on the nature of their protolith and their genesis [50,51]. The Early and Middle Jurassic granitoids in the Chaihe area do not contain primary muscovite. The dark minerals in them include augite, hornblende, and biotite, with the mineral assemblage exhibiting the characteristics of I-type granitoids. Regarding the major element characteristics, the Early-Middle Jurassic granitoids samples are meta-aluminous to weakly peraluminous, with an A/CNK ratio of less than 1.1. Moreover, there is a negative correlation between the P_2O_5 and SiO_2 contents, as shown in the Harker diagram. CIPW-normalized corundum content is less than 1.0 vol%. These characteristics are inconsistent with those of S-type granitoids. In the discrimination diagram for the SiO_2-K_2O rock series, the granitoids samples all fall into the zone of the high-K calc-alkaline series. In the petrogenetic discrimination diagrams (Figure 10) [52], the Early Jurassic granitoids samples mostly fall into the zone of unfractionated granitoids, and the Middle Jurassic granitoids samples are all projected onto the zone of fractionated granitoids.

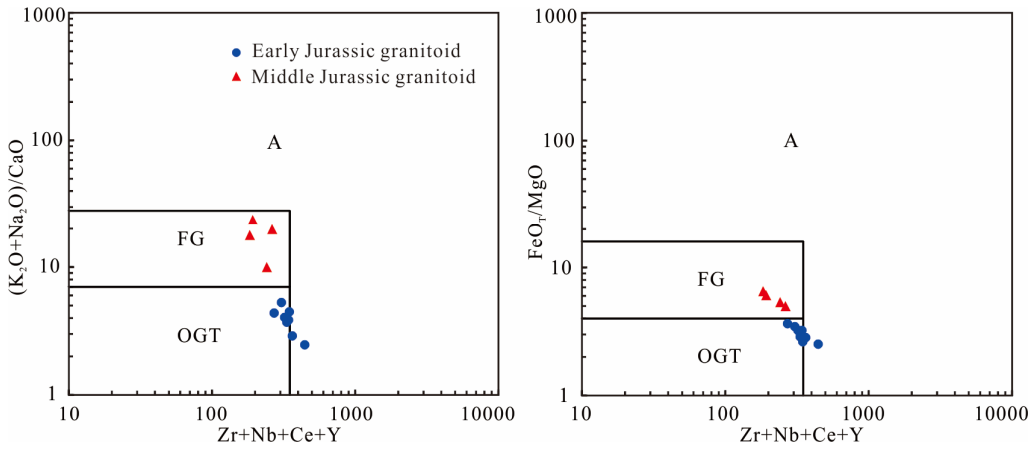

Figure 10. Petrogenetic discrimination diagrams for the Early and Middle Jurassic granitoids in the Chaihe area. FG—fractionated granitoid; OGT—unfractionated granitoid; A—A-type granitoid.

The early crystallization temperature of magmas can be estimated using a zircon saturation thermometer, and accordingly, the formation temperature of granitoids can be obtained [53]. The calculational equation is as follows:

$$T_{Zr}(^{\circ}C) = \{10{,}108/[0.32 + 1.16M + \ln(500{,}000/Zr_{melt})]\} - 273.15$$

where M = (2Ca + K + Na)/(Si × Al) (mole fraction was set at Si + Al + Fe + Mg + Ca + Na + K + P = 1), and Zr_{melt} is approximately replaced with the whole-rock Zr content.

As shown by the calculation results, the Early and Middle Jurassic granitoids in the Chaihe area have an average zircon saturation temperature of about 750 °C and 725 °C, respectively, both of which are lower than the primitive magma temperature of A-type granitoids (generally >830 °C) and approximate the primitive magma temperature of I-type granitoids [54,55]. The zircon saturation temperature of the Middle Jurassic granitoids is about 25 °C less than that of the Early Jurassic granitoids on average, implying that the formation of the Middle Jurassic granitoids might be related to fluid mixing [56]. To sum up, The Early and Middle Jurassic granitoids are high-K calc-alkaline I-type granitoids.

5.2.2. Magma Source

The origin of the granitic magmas has been more of a matter of debate, including: (1) fractional crystallization of mantle-derived basaltic magmas [57,58]; (2) mixing of crust and mantle-derived components [59]; (3) partial melting of an infracrustal source [55,60]. The Chaihe area does not contain associated mafic rocks, which suggests that these Early and Middle Jurassic granitoids were not generated by fractional crystallization of a parental basaltic magma. In addition, the mixing of crust- and mantle-derived melts would generate rocks containing mafic enclaves, whereas samples from the study area are free of mafic enclaves. The ratio of incompatible elements with similar properties can represent the characteristics of the magma source because they are consistent with the source region in the partial melting process and are not affected by fractional crystallization. First, the average Nb/Ta and Ce/Pb ratios of Early and Middle Jurassic granitoids are 12.78 and 3.42, respectively, which are similar to the average crust values [61,62]. Then, the Early Jurassic granitoids have a Zr/Hf ratio of 31.33–35.28 (except for a value of 15.59), which is also similar to the average Zr/Hf ratio (33) of the crust [63]. In contrast, the Middle Jurassic granitoids have a significantly lower Zr/Hf ratio of 16.13–26.20, suggesting that the magma source was mixed with another component during the Middle Jurassic. Compared with the Early Jurassic granitoids, the Middle Jurassic granitoids have a significantly higher Th content, which implies that the magma source might have been contaminated by subduction fluids or ocean-floor sediments during the Middle Jurassic [64,65]. As a result, the Early and Middle Jurassic granitoids should be derived from the partial melting of a crustal source; subsequently, another component was added to the magma source during the Middle Jurassic. This conclusion is also supported by the Hf isotopic composition of zircons. The Early and Middle Jurassic granitoids in the Chaihe area have positive zircon $\varepsilon_{Hf}(t)$ values (+5.64~+14.06) and T_{DM2} (Hf) ages dominated by the Neoproterozoic-Paleozoic, indicating that their magmas are likely to have originated from the partial melting of the lower crustal materials that were newly accreted from the depleted mantle, which is consistent with the Sr-Nd isotopic feature of contemporaneous granitoids in Northeast China [66]. Moreover, the Middle Jurassic granitoids have higher zircon $\varepsilon_{Hf}(t)$ values and approach the depleted mantle evolution line (Figure 5), suggesting that the magma source might be injected with mantle-derived materials, which might be the fluid-metasomatized mantle wedge caused by the dehydration of subducted slabs during the Middle Jurassic.

5.2.3. Magma Evolution

The Early and Middle Jurassic granitoids exhibit a generally linear trend between SiO_2 and other oxide contents (Figure 8). These geochemical variations can be attributed to mineral fractional crystallization during magma processes. First, the decreases in CaO, MgO, and FeO^T with an increase in SiO_2 content can be attributed to fractional crystallization of mafic minerals such as biotite and hornblende. Second, separation of accessory minerals such as apatite and Fe–Ti oxides may be responsible for the observed reductions in P_2O_5 and TiO_2 with increasing SiO_2 content (Figure 8). Third, plagioclase fractional crystallization could explain the decreases in Al_2O_3 and CaO contents as well as the increasingly negative Eu anomalies (Figure 9b). In addition, the Middle Jurassic granitoids have lower Ba, Sr, P, and Ti contents and more obvious negative Eu anomalies than the Early

Jurassic granitoids (Figure 9). Taken together, the Early and Middle Jurassic granitoids have experienced various degrees of fractional crystallization during magma processes.

5.3. Tectonic Setting for the Formation of the Early and Middle Jurassic Granitoids and Its Constraints on the Southward Subduction of the Mongol-Okhotsk Oceanic Plate

The Early and Middle Jurassic granitoids in the study area are composed mainly of quartz monzonites, granodiorites, and monzogranites. They are high-K calc-alkaline series, and these TTGG-like (tonalities, trondhjemites, granodiorites, and granites) rock assemblage characteristics indicate that they might have been formed in a subduction zone environment [67]. As shown in the tectonic-setting discrimination diagram for trace elements (Figure 11a,b) [68], all the Early and Middle Jurassic granitoids plot in the volcanic arc granite field. In the Rb-Hf-Ta discrimination diagram (Figure 11c) [69], the Early Jurassic granitoids also have the characteristics of volcanic arc granites, while the Middle Jurassic granitoids tend to be collisional granites, with some samples falling into the zone of collisional granites. This result indicates that oceanic crust subduction intensified during the Middle Jurassic. The trace element characteristics also indicate that the formation of the Early and Middle Jurassic granitoids was related to the subduction of oceanic crust. In the tectonic-setting discrimination diagram for $FeO_T/(FeO_T + MgO)$-SiO_2 (Figure 11d) [43], all the Early Jurassic granitoids samples fall into the zone of arc-related granitoids, while the Middle Jurassic granitoids samples fall into the zone of post-orogenic granites. Based on these characteristics, it can be inferred that the Early and Middle Jurassic granitoids in the Chaihe area might have been formed in a tectonic setting where subduction transitioned to collision and collision began during the Middle Jurassic.

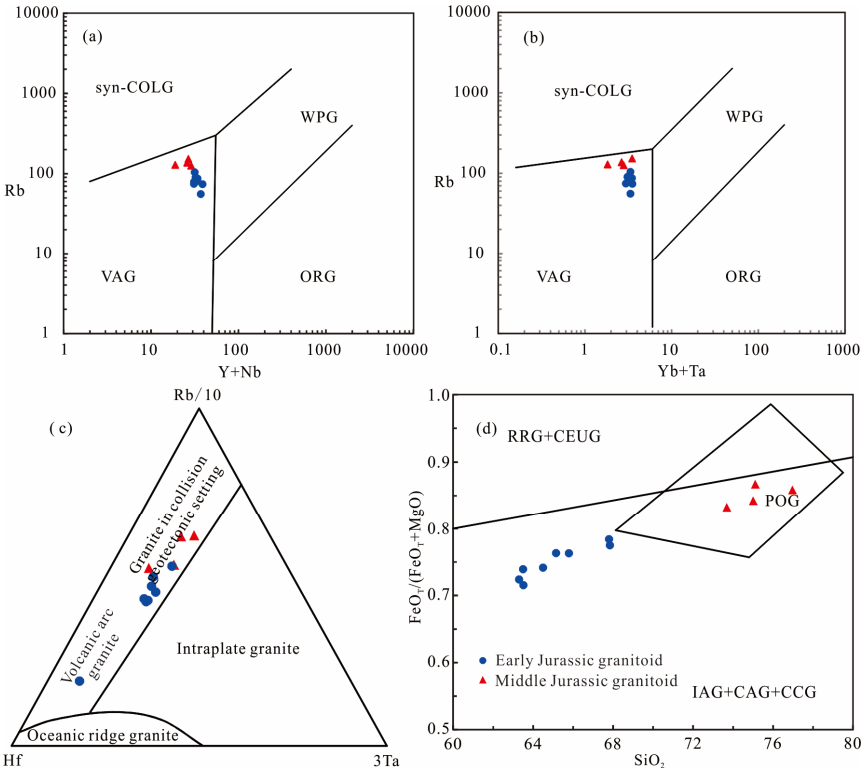

Figure 11. Tectonic-setting discrimination diagrams for the Early and Middle Jurassic granitoids in the Chaihe area. (**a**) Rb-(Y + Nb) diagram [68]; (**b**) Rb-(Yb + Ta) diagram [68]; (**c**) Rb-Hf-Ta diagram [69]; (**d**) $FeO_T/(FeO_T + MgO)$-SiO_2 diagram [43]. ORG—ocean ridge granites; VAG—volcanic arc granites; WPG—within plate granites; syn-COLG—syn-collision granites; IAG—island arc granites; CAG—continental arc granites; CCG—continental collision granites; POG—post-orogenic granites; RRG—rift-related granites; CEUG—continental epeirogenic uplift granites.

Presently, it is primarily believed that the formation of the Mesozoic magmatic rocks in the Great Xing'an Range is related to the closure and post-orogenic collapse of the Mongol-Okhotsk Ocean [24,25], or the subduction of the Paleo-Pacific plate [26], or both [27]. The subduction of the Paleo-Pacific plate beneath the Eurasian continent began during the Early Jurassic, and the influence of subduction extended to the east of the Songliao Basin in northeast China [20,32,70]. Meanwhile, Late Jurassic magmatic activity in northeast China mainly occurred in the Great Xing'an Range and Manzhouli areas to the west of the Songliao Basin but was absent in the Songliao Basin and the eastern areas of Jilin and Heilongjiang. Therefore, the formation of the Early and Middle Jurassic granitoids in the study area might be independent of the subduction of the Paleo-Pacific plate but is more likely to be related to the closure of the Mongol-Okhotsk Ocean.

The Mongol-Okhotsk suture belt, located primarily within Mongolia and Russia, is a suture belt with a long geological history between the Siberian plate and northeast China. It is generally believed that the Mongol-Okhotsk Ocean was broad at the end of the Late Paleozoic [71]. From the Late Triassic onward, this ocean underwent a scissor-like closure from west to east, with its western part closing during the Late Triassic and its eastern part closing from the Late Jurassic possibly until the Early Cretaceous [72–75]. Previous studies mostly focused on the northward subduction of the Mongol-Okhotsk oceanic plate beneath the Siberian plate, but there is a lack of studies on the southward subduction of this oceanic plate. In recent years, increasing numbers of geologists have paid their attention to the southward subduction of the Mongol-Okhotsk oceanic plate. According to the Mongolian terrane division scheme, Permian-Triassic accreted terranes exist on the south side of the Mongol-Okhotsk suture belt, implying that the Mongol-Okhotsk Ocean was subducted southward during the Permian-Triassic [76]. Through the investigation of the Triassic-Jurassic magmatic rocks exposed in the Eerguna block, Chinese geologists confirmed the southward subduction of the Mongol-Okhotsk oceanic plate beneath the Eerguna block [32,77,78]. Therefore, the formation of the Early and Middle Jurassic granitoids in the study area is related to the subduction environment of the oceanic crust, in which the Mongol-Okhotsk oceanic plate was subducted southward beneath the Eerguna and Xing'an blocks. Moreover, the Siberian plate began to collide and converge with the central Great Xing'an Range in northeast China during the Middle Jurassic. This study also indicates that the southern subduction of the Mongol-Okhotsk oceanic plate at least affected the eastern margin of the Xing'an block.

6. Conclusions

(1) The Early and Middle Jurassic granitoids in the Chaihe area are composed mainly of quartz monzonites, granodiorites, and monzogranites. Zircon U–Pb dating of these granitoids indicates that they were formed in 179–172 Ma.

(2) The Early and Middle Jurassic granitoids are high-K calc-alkaline unfractionated I-type granitoids and high-K calc-alkaline fractionated I-type granitoids, respectively. They were derived from the partial melting of newly accreted lower crustal basaltic rocks. Meanwhile, the Middle Jurassic magma sources were mixed with mantle-derived materials, which might be related to the partial melting of mantle wedges caused by the dehydration and metasomatism of subducted slabs.

(3) They were formed in the subduction environment of the oceanic crust, in which the Mongol-Okhotsk oceanic plate was subducted southward beneath the Eerguna and Xing'an blocks.

Supplementary Materials: The following supporting information can be downloaded at: https://www.mdpi.com/article/10.3390/min13070917/s1, Table S1: LA-ICP-MS zircon U-Pb dating results for the Early and Middle Jurassic granitoids in the Chaihe area; Table S2: Results from the Zircon Hf isotope analysis of the Early and Middle Jurassic granitoids in the Chaihe area; Table S3: Analytical results of the major (wt%) and trace (μg/g) element contents of the Early and Middle Jurassic granitoids in the Chaihe area.

Author Contributions: Conceptualization, L.S. and N.J.; methodology, C.Z.; software, Y.F.; validation, Y.W. and X.L.; formal analysis, L.S.; investigation, C.Z.; resources, C.Z.; data curation, Y.F.; writing—original draft preparation, L.S. and N.J.; writing—review and editing, Y.F. and C.Z.; visualization, Y.W. and X.L.; supervision, L.S.; project administration, C.Z.; funding acquisition, N.J. and C.Z. All authors have read and agreed to the published version of the manuscript.

Funding: This research was funded by the National Natural Science Foundation of China (42102087, U2244201, 42172024), the China Postdoctoral Science Foundation (2022M712966), and the Project of China Geological Survey (1212011120654).

Data Availability Statement: The authors confirm that the data generated or analyzed during this study are provided in full within the published article.

Acknowledgments: We thank Academic Editor and three anonymous reviewers whose constructive comments and suggestions greatly improved this manuscript.

Conflicts of Interest: The authors declare no conflict of interest.

References

1. Sengör, A.M.C.; Natal'in, B.A.; Burtman, V.S. Evolution of the Altaid tectonic col-lage and Palaeozoic crustal growth in Eurasia. *Nature* **1993**, *364*, 299–307. [CrossRef]
2. Mossakovsky, A.A.; Ruzhentsev, S.V.; Samygin, S.G.; Kheraskova, T.N. Central Asian fold belt: Geodynamic evolution and formation history. *Geotectonics* **1994**, *24*, 445–474.
3. Xiao, W.J.; Windley, B.F.; Hao, J.; Zhai, M.G. Accretion leading to collision and the Permian Solonker suture, Inner Mongolia, China: Termination of the central Asian oro-genic belt. *Tectonics* **2003**, *22*, 1069. [CrossRef]
4. Jahn, B.M. The Central Asian Orogenic Belt and growth of the continental crust in the Phanerozoic. In *Aspects of the Tectonic Evolution of China*; Malpas, J., Fletcher, C.J.N., Ali, J.R., Aitchison, J.C., Eds.; Geological Society: London, UK, 2004; Volume 226, pp. 73–100. [CrossRef]
5. Kovalenko, V.I.; Yarmolyuk, V.V.; Kovach, V.P.; Kotov, A.B.; Kozakov, I.K.; Salni-kova, E.B.; Larin, A.M. Isotope provinces, mechanisms of generation and sources of the continental crust in the Central Asian mobile belt: Geological and isotopic evidence. *J. Asian Earth Sci.* **2004**, *23*, 605–627. [CrossRef]
6. Windley, B.F.; Alexeiev, D.; Xiao, W.J.; Kröner, A.; Badarch, G. Tectonic models for accretion of the Central Asian orogenic belt. *J. Geol. Soc.* **2007**, *164*, 31–47. [CrossRef]
7. Eizenhöfer, P.R.; Zhao, G.C.; Zhang, J.; Sun, M. Timing of final closure of the Paleo-Asian Ocean along the Solonker Suture Zone: Constraints from the provenance analysis of detrital zircons from Permian sedimentary rocks. *Tectonics* **2014**, *33*, 441–463. [CrossRef]
8. Xiao, W.J.; Santosh, M. The western Central Asian orogenic belt: A window to ac-cretionary orogenesis and continental growth. *Gondwana Res.* **2014**, *25*, 1429–1444. [CrossRef]
9. Cai, K.D.; Sun, M.; Yuan, C.; Zhao, G.C.; Xiao, W.J.; Long, X.P.; Wu, F.Y. Geochronological and geochemical study of mafic dykes from the northwest Chinese Altai: Implications for petrogenesis and tectonic evolution. *Gondwana Res.* **2010**, *18*, 638–652. [CrossRef]
10. Cai, K.D.; Sun, M.; Yuan, C.; Zhao, G.C.; Xiao, W.J.; Long, X.P. Keketuohai mafic–ultramafic complex in the Chinese Altai, NW China: Petrogenesis and geodynamic sig-nificance. *Chem. Geol.* **2012**, *294–295*, 26–41. [CrossRef]
11. Cai, K.D.; Sun, M.; Buslov, M.M.; Yuan, C.; Zhao, G.C.; Long, X.P. Zircon U–Pb geochronology and Hf isotopic composition of granitoids in Russian Altai Mountain, Central Asian Orogenic Belt. *Am. J. Sci.* **2014**, *314*, 580–612. [CrossRef]
12. Geng, H.Y.; Sun, M.; Yuan, C.; Zhao, G.C.; Xiao, W.J. Geochemical and geochronological study of early Carboniferous volcanic rocks from the West Junggar: Petrogenesis and tectonic implications. *J. Asian Earth Sci.* **2011**, *42*, 854–866. [CrossRef]
13. Jiang, Y.D.; Sun, M.; Zhao, G.C.; Yuan, C.; Xiao, W.J.; Xia, X.P.; Long, X.P.; Wu, F.Y. Precambrian detrital zircons in the early Paleozoic Chinese Altai: Their provenance and implications for the crustal growth of central Asia. *Precambr. Res.* **2011**, *189*, 140–154. [CrossRef]
14. Yuan, C.; Sun, M.; Xu, Y.G.; Zhao, G.C.; Xiao, W.J.; Long, X.P.; Yin, J.Y. Oceanic lithospheric mantle beneath the continental crust of the Chinese Altai. *J. Geol. Soc.* **2011**, *168*, 995–1000. [CrossRef]
15. Zhang, J.E.; Xiao, W.J.; Han, C.M.; Ao, S.J.; Yuan, C.; Sun, M.; Geng, H.Y.; Zhao, G.C.; Guo, Q.Q.; Ma, C. Kinematics and age constraints of deformation in a Late Carboniferous accretionary complex in Western Junggar, NW China. *Gondwana Res.* **2011**, *19*, 958–974. [CrossRef]
16. Guo, F.; Li, H.X.; Fan, W.M.; Li, J.Y.; Zhao, L.; Huang, M.W.; Xu, W.L. Early Jurassic subduction of the Paleo-Pacific Ocean in NE China: Petrologic and geochemical evidence from the Tumen mafic intrusive complex. *Lithos* **2015**, *224–225*, 46–60. [CrossRef]
17. Wang, F.; Xu, W.L.; Xing, K.C.; Wang, Y.N.; Zhang, H.H.; Wu, W.; Sun, C.Y.; Ge, W.C. Final Closure of the Paleo-Asian Ocean and Onset of Subduction of Paleo-Pacific Ocean: Constraints From Early Mesozoic Magmatism in Central Southern Jilin Province, NE China. *J. Geophys. Res. Solid Earth* **2019**, *124*, 2601–2622. [CrossRef]

18. Zhang, B.; Guo, F.; Zhang, X.B.; Wu, Y.M.; Wang, G.Q.; Zhao, L. Pacific Ocean in the coastal region of SE China: Petrological and geochemical constraints from the mafic intrusions. *Lithos* **2019**, *334–335*, 8–24. [CrossRef]
19. Li, Z.Q.; Chen, J.L.; Zou, H.; Wang, C.S.; Meng, Q.A.; Liu, H.L.; Wang, S.Z. Mesozo-ic–Cenozoic tectonic evolution and dynamics of the Songliao Basin, NE Asia: Implica-tions for the closure of the Paleo-Asian Ocean and Mongol-Okhotsk Ocean and subduction of the Paleo-Pacific Ocean. *Earth Sci. Rev.* **2021**, *218*, 103471. [CrossRef]
20. Wu, F.Y.; Sun, D.Y.; Ge, W.C.; Zhang, Y.B.; Grant, M.L.; Wilde, S.A.; Jahn, B.M. Geochronology of the Phanerozoic Granitoids in Northeastern China. *J. Asian Earth Sci.* **2011**, *41*, 1–30. [CrossRef]
21. Shi, L.; Zheng, C.; Yao, W.; Li, J.; Cui, F.; Gao, F.; Gao, Y.; Xu, J.; Han, X. Geochronological framework and tectonic setting of the granitic magmatism in the Chaihe–Moguqi region, central Great Xing'an Range, China. *J. Asian Earth Sci.* **2015**, *113*, 443–453. [CrossRef]
22. Yang, W.B.; Niu, H.C.; Cheng, L.R.; Shan, Q.; Li, N.B. Geochronology, geochemistry and geodynamic implications of the Late Mesozoic volcanic rocks in the southern Great Xing'an Mountains, NE China. *J. Asian Earth Sci.* **2015**, *113*, 454–470. [CrossRef]
23. Ge, W.C.; Lin, Q.; Sun, D.Y.; Wu, F.Y.; Won, C.K.; Lee, M.W.; Jin, M.S.; Yun, S.H. Geochemical Characteristics of the Mesozoic Basalts in Da Hinggan Ling: Evidence of the Mantle-crust Interaction. *Acta Petrol. Sin.* **1999**, *15*, 397–407. (In Chinese with English Abstract)
24. Fan, W.M.; Guo, F.; Wang, Y.J.; Lin, G. Late Mesozoic Calcalkaline Volcanism of Post-orogenic Extension in the Northern Da Hinggan Mountains, Northeastern China. *J. Volcanol. Geotherm. Res.* **2003**, *121*, 115–135. [CrossRef]
25. Meng, Q.R. What drove Late Mesozoic Extension of the Northern China-Mongolia Tract? *Tectonophysics* **2003**, *369*, 155–174. [CrossRef]
26. Zhang, J.H.; Gao, S.; Ge, W.C.; Wu, F.Y.; Yang, J.H.; Wilde, S.A.; Li, M. Geochronology of the Mesozoic Volcanic Rocks in the Great Xing'an Range, Northeastern China: Implications for Subduction-induced Delamination. *Chem. Geol.* **2010**, *276*, 144–165. [CrossRef]
27. Wang, F.; Zhou, X.H.; Zhang, L.C.; Ying, J.F.; Zhang, Y.T.; Wu, F.Y.; Zhu, R.X. Late Mesozoic Volcanism in the Great Xing'an Range (NE China): Timing and Implications for the Dynamic Setting of NE Asia. *Earth Planet. Sci. Lett.* **2006**, *251*, 179–198. [CrossRef]
28. Ying, J.F.; Zhou, X.H.; Zhang, L.C.; Wang, F. Geochronological Framework of Mesozoic Volcanic Rocks in the Great Xing'an Range, NE China, and Their Geodynamic Implications. *J. Asian Earth Sci.* **2010**, *39*, 786–793. [CrossRef]
29. Wu, F.Y.; Jahn, B.M.; Wilde, S.A.; Lo, C.H.; Yui, T.F.; Lin, Q.; Ge, W.C.; Sun, D.Y. Highly Fractionated I-type Granites in NE China (I): Geochronology and petrogenesis. *Lithos* **2003**, *66*, 241–273. [CrossRef]
30. Liu, H.; Li, Y.; He, H.; Huangfu, P.; Liu, Y. Two-phase southward subduction of the Mongol-Okhotsk oceanic plate constrained by Permian-Jurassic granitoids in the Erguna and Xing'an massifs (NE China). *Lithos* **2018**, *304–307*, 347–361. [CrossRef]
31. Zhang, S.H.; Zhao, Y.; Song, B.; Hu, J.M.; Liu, S.W.; Yang, Y.H.; Chen, F.K.; Liu, X.M.; Liu, J. Contrasting Late Carboniferous and Late Permian-Middle Triassic Intrusive Suites from the Northern Margin of the North China Craton: Geochronology, Petrogenesis, and Tectonic Implications. *Geol. Soc. Am. Bull.* **2009**, *121*, 181–200. [CrossRef]
32. Xu, W.L.; Pei, F.P.; Wang, F.; Meng, E.; Ji, W.Q.; Yang, D.B.; Wang, W. Spatial–temporal Relationships of Mesozoic Volcanic Rocks in NE China: Constraints on Tectonic Overprinting and Transformations Between Multiple Tectonic Regimes. *J. Asian Earth Sci.* **2013**, *74*, 167–193. [CrossRef]
33. Shi, L.; Tang, Z.; Zheng, C.Q.; Qin, T.; Zhang, L.D.; Wang, Y.; Qian, C.; Yang, F. Genesis and Tectonic Significance of Late Jurassic Granitoids in Chaihe Region, Central Great Xing'an Range, NE China. *J. Jilin Univ.* **2020**, *50*, 112–128. (In Chinese with English Abstract)
34. Geng, J.Z.; Li, H.K.; Zhang, J.; Zhou, H.Y.; Li, H.M. Zircon Hf Isotope Analysis by Means of LA-MC-ICP-MS. *Geol. Bull. China* **2011**, *30*, 1508–1513. (In Chinese with English Abstract)
35. Scherer, E.E.; Munker, C.; Mezger, K. Calibration of the Lutetium–Hafnium clock. *Science* **2001**, *293*, 683–687. [CrossRef]
36. Griffin, W.L.; Pearson, N.J.; Belousova, E.; Jackson, S.V.; Van Achterbergh, E.; O'Reilly, S.Y.; Shee, S.R. The Hf Isotope Composition of Cratonic Mantle: LAM-MC-ICPMS Analysis of Zircon Megacrysts in Kimberlites. *Geochim. Cosmochim. Acta* **2000**, *64*, 133–147. [CrossRef]
37. Nowell, G.M.; Kempton, P.D.; Noble, S.R.; Fitton, J.G.; Saunders, A.D.; Mahoney, J.J.; Taylor, R.N. High Precision Hf Isotope Measurements of MORB and OIB by Thermal Ionization Mass Spectrometry: Insights Into the Depleted Mantle. *Chem. Geol.* **1998**, *149*, 211–233. [CrossRef]
38. Amelin, Y.; Lee, D.C.; Halliday, A.N. Early–middle Archaean Crustal Evolution Deduced from Lu–Hf and U–Pb Isotopic Studies of Single Zircon Grains. *Geochim. Cosmochim. Acta* **2000**, *64*, 4205–4225. [CrossRef]
39. Li, X.H.; Li, Z.X.; Zhou, H.W.; Liu, Y.; Kinny, P.D. U-Pb zircon geochronology, geochemistry and Nd isotopic study of Neoproterozoic bimodal volcanic rocks in the Kangdian rift of South China: Implications for the initial rifting of Rodinia. *Precambrian Res.* **2002**, *113*, 135–154. [CrossRef]
40. Yang, J.H.; Wu, F.Y.; Shao, J.A.; Wilde, S.A.; Xie, L.W.; Liu, X.M. Constraints on the Timing of Uplift of the Yanshan Fold and Thrust Belt, North China. *Earth Planet. Sci. Lett.* **2006**, *246*, 336–352. [CrossRef]
41. Peccerillo, A.; Taylor, S.R. Geochemistry of Eocene calc-alkaline volcanic rocks from the Kastamonu area, Northern Turkey. *Contrib. Miner. Petrol.* **1976**, *58*, 63–81. [CrossRef]
42. Middlemost, E.A. *Magmas and Magmatic Rocks*; Longman: London, UK, 1985; pp. 1–266.
43. Maniar, P.D.; Piccoli, P.M. Tectonic discrimination of granitoids. *Geol. Soc. Am. Bull.* **1989**, *101*, 635–643. [CrossRef]

44. Middlemost, E.A. Naming materials in the magma/igneous rock system. *Earth Sci. Rev.* **1994**, *37*, 215–224. [CrossRef]
45. Irvine, T.N.; Baragar, W.R.A. A Guide to the Chemical Classification of the Common Volcanic Rocks. *Can. J. Earth Sci.* **1971**, *8*, 523–548. [CrossRef]
46. Sun, S.; McDonough, W.F. Chemical and isotopic systematics of oceanic basalts: Implications for mantle composition and processes. *Geol. Soc. Lond. Spec. Publ.* **1989**, *42*, 313–345. [CrossRef]
47. Gao, F.; Xu, W.; Yang, D.; Pei, F.; Liu, X.; Hu, Z. LA-ICP-MS Zircon U–Pb Dating from Granitoids in Southern Basement of Songliao Basin: Constraints on Ages of the Basin Basement. *Sci. China Ser. D Earth Sci.* **2007**, *50*, 995–1004. [CrossRef]
48. Ge, W.C.; Wu, F.Y.; Zhou, C.Y.; Zhang, J.H. Zircon U-Pb Ages and Its Significance of the Mesozoic Granites in the Wulanhaote Region, Central Da Hinggan Mountain. *Acta Petrol. Sin.* **2005**, *21*, 749–762. (In Chinese with English Abstract)
49. Yu, H.C.; He, Z.H.; Sui, Z.M.; Dong, Y.; Zhu, K. Determination and geological implication of the Middle Jurassic postcollisional granitoids in Taerqi area, central Great Xing'an Range. *Acta Petrol. Sin.* **2020**, *36*, 3721–3740. (In Chinese with English Abstract) [CrossRef]
50. Chappell, B.W.; White, A.J.R. Two constrasting granite types. *Pac. Geol.* **1974**, *8*, 173–174.
51. Zhao, K.D.; Jiang, S.Y.; Yang, S.Y.; Dai, B.Z.; Lu, J.J. Mineral chemistry, trace elements and Sr-Nd-Hf isotope geochemistry and petrogenesis of Cailing and Furong granites and mafic enclaves from the Qitianling batholith in the Shi-Hang zone. South China. *Gondwana Res.* **2012**, *22*, 310–324. [CrossRef]
52. Whalen, J.B.; Currie, K.L.; Chappell, B.W. A-type Granites: Geochemical Characteristics, Discrimination and Petrogenesis. *Contrib. Mineral. Petrol.* **1987**, *95*, 407–419. [CrossRef]
53. Boehnke, P.; Watson, E.B.; Trail, D.; Harrison, T.M.; Schmitt, A.K. Zircon saturation re-revisited. *Chem. Geol.* **2013**, *351*, 324–334. [CrossRef]
54. Clemens, J.D.; Holloway, J.R.; White, A.J.R. Origin of an A-type granite: Experimental constraints. *Am. Mineral.* **1986**, *71*, 317–324.
55. King, P.L.; White, A.J.R.; Chappell, B.W.; Allen, C.M. Characterization and Origin of Aluminous A-type Granites from the Lachlan Fold Belt, Southeastern Australia. *J. Petrol.* **1997**, *38*, 371–391. [CrossRef]
56. Wu, F.Y.; Li, X.H.; Yang, J.H.; Zheng, Y.F. Discussions on the Petrogenesis of Granites. *Acta Petrol. Sin.* **2007**, *23*, 1217–1238. (In Chinese with English Abstract)
57. Eby, G.N.; Woolley, A.R.; Din, V.I.C.; Platt, G. Geochemistry and Petrogenesis of Nepheline Syenites: Kasungu–Chipala, Ilomba, and Ulindi Nepheline Syenite Intrusions, North Nyasa Alkaline Province, Malawi. *J. Petrol.* **1998**, *39*, 1405–1424. [CrossRef]
58. Litvinovsky, B.A.; Jahn, B.M.; Eyal, M. Mantle-derived sources of syenites from the A-type igneous suites—New approach to the provenance of alkaline silicic magmas. *Lithos* **2015**, *232*, 242–265. [CrossRef]
59. Mingram, B.; Trumbull, R.B.; Littman, S.; Gerstenberger, H. A petrogenetic study of anorogenic felsic magmatism in the Cretaceous Paresis ring complex, Namibia: Evidence for mixing of crust and mantle-derived components. *Lithos* **2000**, *54*, 1–22. [CrossRef]
60. Martin, R.F. A-type granites of crustal origin ultimately result from open-system fenitization-type reactions in an extensional environment. *Lithos* **2006**, *91*, 125–136. [CrossRef]
61. Barth, M.G.; McDonough, W.F.; Rudnick, R.L. Tracking the budget of Nb and Ta in the continental crust. *Chem. Geol.* **2000**, *165*, 197–213. [CrossRef]
62. Rudnick, R.L.; Fountain, D.M. Nature and composition of the continental crust: A lower crustal perspective. *Rev. Geophys.* **1995**, *33*, 267–309. [CrossRef]
63. Taylor, S.R.; Mclennan, S.M. *The Continental Crust: Its Composition and Evolution*; Blackwell Scientific Publish: Hoboken, NJ, USA, 1985.
64. Othman, D.B.; White, W.M.; Patchett, J. The Geochemistry of Marine Sediments, Island Arc Magma Genesis, and Crust-mantle Recycling. *Earth Planet. Sci. Lett.* **1989**, *94*, 1–21. [CrossRef]
65. Plank, T.; Langmuir, C.H. The Chemical Composition of Subducting Sediment and Its Consequences for the Crust and Mantle. *Chem. Geol.* **1998**, *145*, 325–394. [CrossRef]
66. Wu, F.Y.; Sun, D.Y.; Lin, Q. Petrogenesis of the Phanerozoic Granites and Crustal Growth in Northeast China. *Acta Petrol. Sin.* **1999**, *15*, 181–189. (In Chinese with English Abstract)
67. Liu, J.X.; Liu, C.; Deng, J.F.; Luo, Z.H.; He, G.Q.; Liu, Q. Igneous Records of Mongolia–Okhotsk Ocean Subduction: Evidence from Granitoids in the Greater Khingan Mountains. *Minerals* **2023**, *13*, 493. [CrossRef]
68. Pearce, J.A.; Harris, N.B.W.; Tindle, A.G. Trace Element Discrimination Diagrams for the Tectonic Interpretation of Granitic Rocks. *J. Petrol.* **1984**, *25*, 956–983. [CrossRef]
69. Harris, N.B.W.; Pearce, J.A.; Tindle, A.G. Geochemical Characteristics of Collision-Zone Magmatism//Coward MP, Ries AC. Collision Tectonics. *Geol. Soc. Lond. Spec. Publ.* **1986**, *19*, 67–81. [CrossRef]
70. Tang, J.; Xu, W.; Wang, F.; Ge, W. Subduction History of the Paleo-Pacific Slab Beneath Eurasian Continent: Mesozoic-Paleogene Magmatic Records in Northeast Asia. *Sci. China Earth Sci.* **2018**, *61*, 527–559. [CrossRef]
71. Cogné, J.P.; Kravchinsky, V.A.; Halim, N.; Hankard, F. Late Jurassic-Early Cretaceous Closure of the Mongol-Okhotsk Ocean Demonstrated by New Mesozoic Palaeomagnetic Results from the Trans-Baikal Area (SE Siberia). *Geophys. J. Int.* **2005**, *163*, 813–822. [CrossRef]
72. Zonenshain, L.P.; Kuzmin, M.L.; Natapov, L.M. *Geology of the USSR: A Plate-Tectonics Synthesis*; Geodynamics Series; American Geophysical Union: Washington, DC, USA, 1990; Volume 21, pp. 1–242.

73. Zorin, Y.A. Geodynamics of the Western Part of the Mongolia-Okhotsk Collisional Belt, Trans-Baikal Region (Russia) and Mongolia. *Tectonophysics* **1999**, *306*, 33–56. [CrossRef]
74. Kravchinsky, V.A.; Cogné, J.P.; Harbert, W.P.; Kuzmin, M.I. Evolution of the Mongol-Okhotsk Ocean as Constrained by New Palaeomagnetic Data from the Mongol-Okhotsk Suture Zone, Siberia. *Geophys. J. Int.* **2002**, *148*, 34–57. [CrossRef]
75. Sorokin, A.A.; Yarmolyuk, V.V.; Kotov, A.B.; Sorokin, A.P.; Kudryashov, N.M.; Tzzin'i, L. Geochronology of Triassic-Jurassic Granitoids in the Southern Framing of the Mongol-Okhotsk Fold Belt and the Problem of Early Mesozoic Granite Formation in Central and Eastern Asia. *Dokl. Earth Sci.* **2004**, *399*, 1091–1094.
76. Badarch, G.; Dickson, C.W.; Windley, B.F. A New Terrane Subdivision for Mongolia: Implications for the Phanerozoic Crustal Growth of Central Asia. *J. Asian Earth Sci.* **2002**, *21*, 87–110. [CrossRef]
77. Tang, J.; Xu, W.L.; Wang, F.; Zhao, S.; Wang, W. Early Mesozoic Southward Subduction History of the Mongol–Okhotsk Oceanic Plate: Evidence from Geochronology and Geochemistry of Early Mesozoic Intrusive Rocks in the Erguna Massif, NE China. *Gondwana Res.* **2016**, *31*, 218–240. [CrossRef]
78. Shi, L.; Tang, Z.; Zhang, Y.J.; Yang, L. Sedimentary environment and geochemistry of the Middle Jurassic Wanbao Formation in Suolun area, middle Daxinganling Mountains. *Geol. Resour.* **2022**, *31*, 579–587+605. (In Chinese with English Abstract) [CrossRef]